In situ labeling of immune cells with iron oxide particles: An approach to detect organ rejection by cellular MRI

Yijen L. Wu, Qing Ye, Lesley M. Foley, T. Kevin Hitchens, Kazuya Sato, John B. Williams, and Chien Ho†

Pittsburgh NMR Center for Biomedical Research, Department of Biological Sciences, Carnegie Mellon University, 4400 Fifth Avenue, Pittsburgh, PA 15213

Edited by Shu Chien, University of California at San Diego, La Jolla, CA, and approved December 9, 2005 (received for review August 18, 2005)

In vivo **cell tracking by MRI can provide means to observe biological processes and monitor cell therapy directly. Immune cells, e.g., macrophages, play crucial roles in many pathophysiological processes, including organ rejection, inflammation, autoimmune diseases, cancer, atherosclerotic plaque formation, numerous neurological disorders, etc. The current gold standard for diagnosing and staging rejection after organ transplantation is biopsy, which is not only invasive, but also prone to sampling errors. Here, we report a noninvasive approach using MRI to detect graft rejection after solid organ transplantation. In addition, we present the feasibility of imaging individual macrophages *in vivo* by MRI in a rodent heterotopic working-heart transplantation model using a more sensitive contrast agent, the micrometer-sized paramagnetic iron oxide particle, as a methodology to detect acute cardiac rejection.**

cardiac rejection | detection of single macrophage | micrometer-sized iron oxide particle | nanometer-sized iron oxide particle

The ability to noninvasively track cell migration, cell homing, and cellular fate *in vivo* is of pivotal importance for understanding the complex roles that different cells play in biology and cellular medicine. Immune cells, such as macrophages, play crucial roles in many pathophysiological processes, including organ rejection, inflammation, autoimmune diseases, and development of coronary heart diseases, as well as numerous neurological disorders. MRI allows noninvasive functional assessment and visualization of anatomy *in vivo* with very high spatial resolution. MRI also has the advantages over other imaging modalities of having excellent soft tissue contrast, no need to administer radioactive isotopes, and good deep tissue penetration. There is rapid growth in using MRI for cellular and molecular imaging. Numerous studies have demonstrated wide applications and great potential impact on biological and medical sciences, including tracking stem cells after transplantation (1–5); repairing myocardial infarction (6), muscular disorders (7), and stroke (8, 9); tracking stem cells in neovasculature of early glioma as a means for cancer detection and gene therapy (10); monitoring inflammation (11, 12); detecting early graft rejection (13); and visualizing gene expression (14, 15). For a recent review, see ref. 16.

Although gadolinium-based contrast agents (17) play an important role in molecular and cellular imaging, most cellular MRI studies rely on the superior relaxivity of superparamagnetic iron oxide (SPIO) or ultra-small superparamagnetic iron oxide (USPIO) nanoparticles for imaging contrast. Cells containing a significant number of these agents are observed by a localized area of hypointensity in T_2^*-weighted MRI images. These contrast agents are composed of an iron oxide core usually with a dextran coating ranging in size from 20 to 30 nm (USPIO) to a few hundred nm (SPIO). Single cells labeled with SPIO or USPIO particles can be visualized with *ex vivo* MRI (18, 19), but not *in vivo*. Recently, it has been reported that, with much larger micrometer-sized spheres containing iron oxide (20, 21), single particles can be visualized by MRI. Referred to here as MPIO (micrometer-sized paramagnetic iron oxide) particles, these particles are highly effective T_2^* contrast agents composed of polystyrene/divinyl benzene polymer microspheres containing a magnetite (iron oxide) core.

In this study, we have explored the possibility of using MRI to noninvasively monitor individual immune cells, primarily macrophages, *in vivo*, after heart and lung transplantation. The gold standard for rejection surveillance after organ transplantation is biopsy, which not only is invasive, but also is prone to sampling errors (22, 23). Therefore, a noninvasive alternative that can complement biopsy is highly desirable. This study employs a rodent heterotopic working-heart and lung transplantation model for studying acute graft rejection (24).

Mammalian cells can be labeled with MRI contrast agents either *ex vivo* or *in vivo* (*in situ*) (13). Specific cell types can be labeled with the *ex vivo* method, in which the cells are isolated, labeled with contrast agent in culture, and then reintroduced back into the body. There are excellent efforts in increasing the cellular loading of MRI contrast agents, including employing transfecting agents (25–28), linking Tat peptide (29, 30), or by receptor-mediated means (31). Alternatively, cells can be labeled *in situ*, in which the contrast agent is administered intravenously. Although only effective for cell types that can readily phagocytose or endocytose the contrast agent, such as macrophages, this labeling method is convenient and potentially more easily applied to a clinical setting. In this study, direct i.v. injection of an MPIO suspension is used for *in vivo* labeling of immune cells to noninvasively monitor organ transplant rejection by using MRI.

Results and Discussion

Immune Cells Can Be Labeled with Iron Oxide Particles *in Vivo* Visualized with MRI. Immune cells, especially macrophages, have been labeled *in vivo* by direct i.v. administration of USPIO particles (13, 32–35). Iron oxide particles can be endocytosed by macrophages in circulation, without needing to isolate cells first, and the labeled macrophages can migrate to the rejecting graft. The infiltration of macrophages labeled with MPIOs at the rejection site can be observed noninvasively with MRI. Discrete, punctate, negative contrast can be readily seen throughout the rejecting allograft heart (Fig. 1 *A*–*C*) and lung (Fig. 1*D*) 1 day after i.v. administration of MPIOs on postoperational day (POD) 5 (Fig. 1*A*) and POD 6 (Fig. 1 *B* and *C*). The high-contrast regions in the allografts seem to be punctate and circular in shape, like spots. Each spot of high contrast with the MPIO labeling most likely indicates one or a few iron-laden macrophages that have infiltrated into the rejection site. The

Conflict of interest statement: No conflicts declared.

This paper was submitted directly (Track II) to the PNAS office.

Abbreviations: SPIO, superparamagnetic iron oxide; USPIO, ultra-small SPIO; MPIO, micrometer-sized paramagnetic iron oxide; POD, postoperational day; LV, left ventricle/ventricular; RV, right ventricle/ventricular; MRM, magnetic resonance microscopy.

†To whom correspondence should be addressed. E-mail: chienho@andrew.cmu.edu.

www.pnas.org/cgi/doi/10.1073/pnas.0507198103

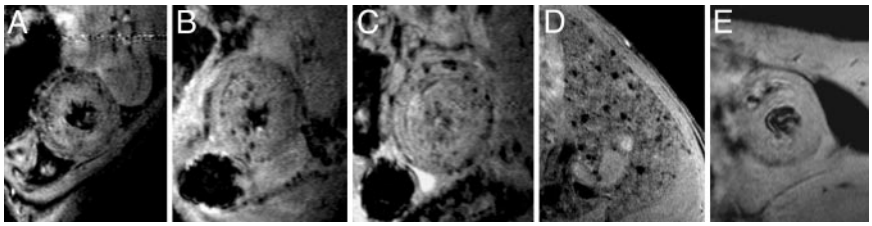

Fig. 1. *In vivo* MRI of allograft hearts and lungs, 1 day after i.v. injection of MPIO particles. (*A*) Allograft heart on POD 5. (*B* and *C*) Allograft heart on POD 6. (*D*) Allograft lung on POD 6. (*E*) Isograft heart on POD 6. Shown with 156-μm in-plane resolution at 4.7 Tesla by using a Bruker Biospec AVANCE-DBX MRI instrument.

area with contrast on POD 5 (Fig. 1*A*) is smaller and more concentrated toward the outer regions of the left-ventricular (LV) wall than that found on POD 6 (Fig. 1 *B* and *C*). The spatial distribution of MPIO-labeled cells is dependent on the degree of rejection. On the contrary, without rejection, no detectable contrast changes are seen in the isograft control (Fig. 1*E*) on POD 6 with the same labeling and imaging conditions.

Longitudinal Study of MPIO-Labeled Macrophages at the Rejection Site *in Vivo*. To investigate the time course of MPIO-labeled macrophages *in vivo*, the same recipient was serially imaged for 3 days after administrating the MPIO on POD 3.5. In a mild rejection stage on POD 3.5, as early as 2 h after the MPIO administration, discrete, punctate spots could be seen in parts of the allograft heart, mainly in the outer regions of the right ventricle (RV) and the pericardium of the LV wall (Fig. 2*A*). This contrast, observed within a few hours after the MPIO administration, likely results from labeled macrophages that are already present at the rejection site at the time of the particle administration. On POD 4.5, with rejection progressing, discrete spots can be seen in the LV and RV walls and are more concentrated in the outer walls (Fig. 2*B*). The areas with iron-laden cells seem to be larger than those observed on POD 3.5. On POD 5.5 (Fig. 2*C*), with more advanced graft rejection, the region of contrast extends throughout the inner part of the LV and RV walls, even though no additional MPIOs have been injected.

Injection of MPIOs on POD 3 allows for repetitive imaging to follow the progression of acute rejection for at least 3 days. Although we have not specifically studied the blood half-life of MPIOs, it is not likely to last more than a day, because the blood half-life of all of the smaller iron oxide-based contrast agents is in the order of minutes to several hours. Thus, it is not likely to have MPIOs in circulation after 1 day postinjection. The progression pattern of the MPIO-labeled immune cells over time correlates well with the progression of the acute rejection in the heart allograft. This result indicates that, once ingested by cells, the MPIOs are stable and can have a lifetime of at least a few days in our rat model. Therefore, MPIO-particle labeling opens the door for detection of individual cells over a longer period. This finding is consistent with that of Shapiro *et al.* (20) that MPIOs can remain in labeled cells after multiple cell divisions.

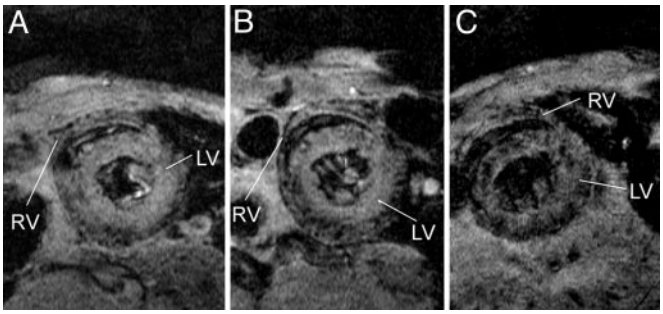

Fig. 2. *In vivo* MRI of a rat allograft heart over time. MPIO particles are administered once on POD 3.5, and the same animal is imaged on POD 3.5 (*A*), 4.5 (*B*), and 5.5 (*C*), with 156-μm in-plane resolution at 4.7 Tesla by using a Bruker Biospec AVANCE-DBX MRI instrument.

As the rejection progresses, it seems to be that more MPIO-labeled macrophages are recruited to the rejection sites. The areas of the myocardium with MPIO-labeled macrophage infiltration are 7.9%, 13.2%, and 36.9% on POD 3.5, 4.5, and 5.5, respectively. It is not clear, however, whether the seemingly increased number of labeled macrophages in the graft is due to migration from circulation, other lymph organs, or due to local proliferation. It is known that local proliferation of macrophages plays an important role during rejection. However, in our case, there is no significant decrease in the contrast-to-noise ratios for the infiltrated areas; i.e., contrast-to-noise ratios are found to be 1.34 ± 0.16, 1.06 ± 0.25, and 1.43 ± 0.23 for POD 3.5, 4.5, and 5.5, respectively. If local proliferation does occur in the rejecting graft, the dilution of the contrast agent does not seem to cause a significant loss in the contrast over the time frame of our measurements. This observation again demonstrates the advantage of the enhanced detectability of MPIO over smaller iron oxide contrast agents.

Although highly punctate, the high-contrast regions seen in Fig. 2*C* (POD 5.5) are not as spot-like and circular in shape as that in Fig. 1 *A–D* (POD 5 and 6). When the concentration of labeled cells is sparse, individual cells are more likely to be resolved. When the concentration of labeled cells increases, the boundaries of cellular contrast radii of background gradient start to overlap, resulting in more patchy contrast pattern.

Our data reveal a pericardium-to-endocardium progression pattern of macrophage infiltration in LV as the rejection progresses. This temporal distribution of the immune-cell infiltration has not been previously demonstrated because biopsy is generally limited to a small inter-cardiac sampling area. Direct imaging of macrophage infiltration with MRI not only is noninvasive, but also provides a whole-heart visualization of cellular infiltration, both in LV and RV. The pericardium-to-endocardium temporal progression pattern of the macrophage infiltration is likely to be a result of rejection rather than other causes, e.g., surgical ischemic insults or inflammation, because no detectable macrophage infiltration is seen in isografts that underwent identical experimental procedures.

Comparable, Yet Distinct, Contrast Pattern by *in Vivo* Labeling of MPIO and USPIO. Previously, we have demonstrated in a nonworking heart and lung model that MRI signal attenuation with USPIO labeling correlates with rejection (33, 34). In our current working-heart model with higher MRI resolution, the distinctive contrast pattern of punctate dots caused by *in vivo* MPIO labeling in the rejecting heart and lung is comparable, yet very different from the contrast pattern observed by using USPIO particles. After *in vivo* labeling with USPIO, infiltration of the

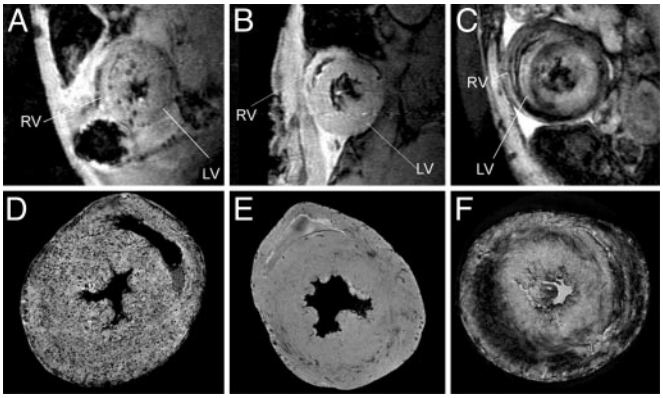

Fig. 3. Contrast patterns labeled with two different contrast agents. (*A–C*) *In vivo* MRI of macrophage accumulation on POD 6 of an allograft heart with MPIO-particle labeling (*A*), an isograft heart with MPIO-particle labeling (*B*), and an allograft heart with USPIO labeling (*C*), with 156-μm in-plane resolution at 4.7 Tesla. (*D–F*) MRM at 11.7 Tesla using a Bruker AVANCE-DBX MRI instrument with in-plane resolution of 40 μm of an allograft heart with MPIO-particle labeling (*D*), an isograft heart (*E*), and an allograft heart with USPIO labeling (*F*). All hearts used in the *in vivo* and *ex vivo* measurements were the same ones except those used in *A* and *D*.

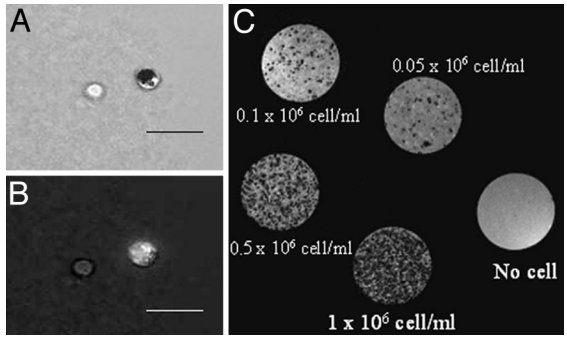

Fig. 4. *Ex-vivo* labeled macrophages. Light microscopy (*A*) and fluorescent microscopy (*B*) of *ex vivo* MPIO-labeled macrophages. (Scale bars: 50 μm.) (*C*) MRM at 11.7-Tesla using a Bruker AVANCE-DBX MRI instrument with in-plane resolution of 40 μm of gelatin phantoms containing isolated macrophages labeled with MPIO particles with different cell concentration.

iron-laden macrophages can also be seen with *in vivo* MRI (Fig. 3*C*). On POD 6, the spatial distribution of iron-laden macrophages at the rejecting allograft hearts is comparable with both MPIO (Fig. 3*A*) and USPIO (Fig. 3*C*) labeling, i.e., both more concentrated at the inner regions of the LV wall. However, the contrast pattern after *in vivo* USPIO labeling (Fig. 3*C*) manifests itself over a large continuous area of contrast and not the punctate pattern as seen with MPIO labeling (Fig. 3*A*). The isograft control (Fig. 3*B*) does not show any detectable contrast after either MPIO or USPIO labeling.

The different contrast patterns can be better depicted with high-resolution magnetic resonance microscopy (MRM) at 11.7 Tesla (Fig. 3 *D–F*). With a 40-μm isotropic resolution, discrete black dots can be seen throughout the excised allograft heart (Fig. 3*D*) after *in vivo* MPIO labeling, and the diameter of the black spots range from 50 to 150 μm. Each spot of hypointensity seems to be discrete and circular, likely resulting from a single macrophage. There appear to be many more spots in *D* than in *A*. The heart in *D* was not the same one used in *A*, and the slice selection for these two cases was not the same. The greater number of spots in *D* could be due to a larger magnetic susceptibility generated at 11.7 Tesla than at 4.7 Tesla. Also, the *in vitro* measurement (*D*) of a fixed heart with higher resolution and no motion is likely to resolve individual MPIO particles inside a macrophage than the *in vivo* experiment (*A*). See Fig. 4*C* for a comparison with gel phantoms containing macrophages labeled with MPIO particles. On the other hand, even with such high resolution, the allografts labeled with USPIO (Fig. 3*F*) still show a continuous contrast pattern, but not the punctate pattern. The isograft control (Fig. 3*E*) does not show contrast patterns that resemble either MPIO or USPIO contrast patterns. Some dark areas seen in the isograft control are the result of blood vessels.

Although MPIO and USPIO cause comparable distribution of labeled cells, the observed contrast patterns are quite different. One possibility is due to a difference in the labeling efficiency as well as the effective concentration of these two particles. In the present study, the MPIO and USPIO doses were chosen such that the same total amount of iron was injected into the animals. Because each MPIO particle contains more iron than that of a USPIO particle, the actual numbers of USPIO particles injected are up to 2 orders of magnitude more than the equivalent of MPIO dose. Therefore, a greater number of macrophages should be labeled with USPIO than with MPIO, and, with USPIO labeling, the cellular boundaries are less likely to be resolved. A similar contrast pattern is also observed when a higher dose of MPIO is given (Fig. 2*C*); i.e., the individual contrast boundaries are not well defined.

***Ex Vivo*-Labeled Isolated Macrophages.** Macrophages were isolated from spleenocytes and labeled *ex vivo* with MPIO to compare the MRI contrast pattern in phantoms with that found for the *in vivo* labeling. With simple incubation in culture, a significant amount of iron uptake can be observed under light microscopy (Fig. 4*A*, right cell). These iron-laden macrophages exhibit bright green fluorescence (Fig. 4*B*, right cell), which indicates up-take of the MPIO particles containing the Dragon Green probe. Most but not all cells are labeled. Cells void of fluorescence (Fig. 4*B*, left cell) are also lacking intercellular iron (Fig. 4*A*, left cell). MRM of gelatin phantoms (Fig. 4*C*) containing isolated MPIO-labeled macrophages shows similar discrete, punctate, high-contrast regions that resemble the contrast pattern of allograft hearts after *in vivo* MPIO labeling (see Fig. 3*D*). At lower cell concentrations (0.05×10^6 cells per ml and 0.1×10^6 cells per ml), individual dark spots can be clearly resolved, the shape of the spots seem to be circular, and the sizes of the dark spots observed in the phantom are similar to the size observed by labeling with MPIO in our rat allograft heart/lung model. This is additional evidence that the discrete, punctate, high-contrast areas seen after *in vivo* MPIO labeling in the allografts are likely to be individual cells. At higher concentrations (0.5×10^6 cells per ml and 1×10^6 cells per ml), although still being discrete and punctate, it becomes harder to resolve contrast boundaries from individual labeled cells. Administration of the *ex vivo*-labeled macrophages led to the contrast patterns similar to those observed with our *in vivo* labeling (results not shown).

Histology of Allograft Hearts After MPIO Labeling. The punctate, contrast pattern caused by MPIO labeling does not appear due to random interstitial deposition of iron oxide particles, but rather to intracellular uptake particles, mainly found in macrophages, not myocytes. Fig. 5 shows histological evaluation of allograft hearts (POD 6) after *in vivo* MPIO labeling. In an area near the pericardium, the iron-containing cells revealed by Prussian blue staining (Fig. 5*A*, blue) correlate with ED1$^+$ macrophages (Fig. 5*B*, brown) in the areas with more aggressive immune cell infiltration and disrupted myocardial integrity as revealed by hematoxylin/eosin (H&E) staining (Fig. 5*C*). Iron appears largely inside ED1$^+$ macrophages, not in myocytes or in random interstitial space. The same phenomenon can be seen in

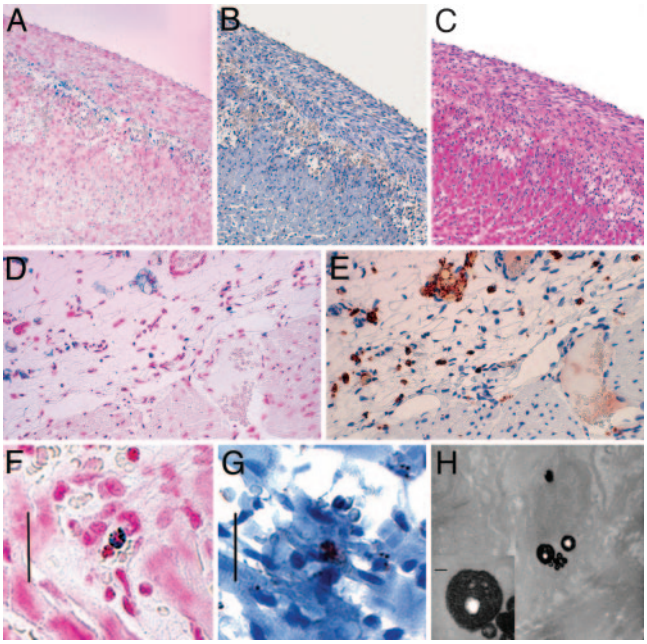

Fig. 5. Histological examination of allograft hearts on POD 6 after *in vivo* MPIO-particle labeling. (*A–C*) Optical micrograph (×200 magnification) of three neighboring 5-μm tissue sections of a POD 6 allograft heart stained with Perl's Prussian blue for iron (*A*, blue; with pink background counterstaining), anti-rat ED1 for macrophage (*B*, brown; with blue background counterstaining), and hematoxylin/eosin staining (*C*) for tissue integrity. (*D* and *E*) Optical micrograph (×400 magnification) of two neighboring 5-μm tissue sections of another POD 6 allograft heart stained with Perl's Prussian blue for iron (*D*, blue; with pink background counterstaining), and anti-rat ED1 for macrophage (*E*, brown; with blue background counterstaining). (*F* and *G*) Partial view of optical micrograph (×400 magnification) of two neighboring 5-μm tissue sections of a POD 6 allograft heart stained with Perl's Prussian blue for iron (*F*, blue; with pink background counterstaining) and anti-rat ED1 for macrophage (*G*, brown; with blue background counterstaining). (Scale bars: 75 μm.) (*H*) Electron micrograph of an allograft heart harvested on POD 6 after *in vivo* MPIO-particle labeling. (*Inset*) Enlarged area. (Scale bar: 100 nm.)

the endocardial region of a different allograft heart, where iron-containing cells (Fig. 5*D*, blue) are all included in ED1$^+$ macrophages (Fig. 5*E*, brown). With higher magnification, several iron-dense pockets can be seen in a single iron-containing cell (Fig. 5*F*), and this cell is an ED1$^+$ macrophage (Fig. 5*G*). Thus, histological examination indicates that iron is contained in intact cells, not in the random interstitial space, and the iron-containing cells largely correlate with ED1$^+$ macrophages.

Multiple iron-dense particles are observed within one cell (Fig. 5*F*), most likely in the cytoplasm. This finding is consistent with electron micrograph (EM) evaluation of an allograft heart (POD 6) after *in vivo* MPIO-particle labeling, which shows that the iron is within the membrane-bound vesicles and multiple MPIO-particle-containing vesicles can often be found in one cell (Fig. 5*H*). Evidently, the number of superparamagnetic particles ingested by a single cell is sufficient to cause detectable water proton signal attenuation in one voxel, so that single cells containing MPIO particles can be detected by MRI *in vivo*.

To confirm that the cells ingesting the MPIO particles are indeed macrophages, anti-ED1 immunofluorescent staining was performed. Fluorescent images were taken on the same sample under the same field of view with a green fluorescence channel for MPIO (Fig. 6*A*) and a red fluorescent channel for ED1 (Fig. 6*B*). The majority of cells that are positive with Dragon Green fluorescence also show red fluorescence. For a direct comparison, three regions are selected with white boxes, and the overlay double fluorescence images are shown on the (Fig. 6, *Right*). The

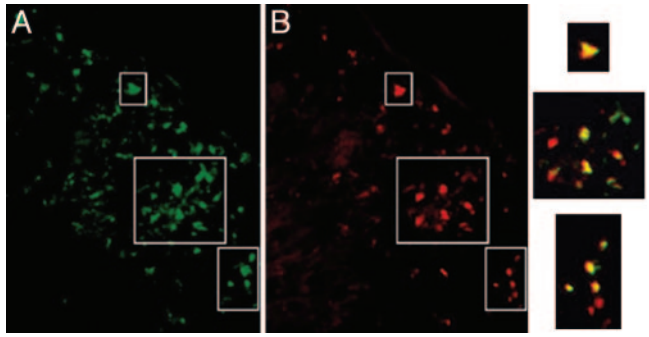

Fig. 6. Double fluorescence for MPIO particles and ED1. Shown are fluorescence microscopy of Dragon green for MPIOs (*A*) and anti-ED1 (red) immunofluorescence microscopy for microphages of the same field of view (*B*). The boxes select three regions for overlaying double fluorescence. The overlay images are enlarged on the *Right*.

cells positive for both green and red fluorescence exhibit yellow color.

Temporal Progression of ED1$^+$ Macrophage Infiltration. Our *in vivo* MRI results show a pericardium-to-endocardium progression pattern of MPIO-labeled macrophages as rejection progresses, which has not been previously observed because biopsy samples are very limited in location and size. Fig. 7 shows anti-rat ED1 staining of allograft hearts on POD 3, 4, 5, and 6. ED1$^+$ cells are stained brown on the blue counterstaining background. On POD 3 (Fig. 7*A*) with only very mild rejection, ED1$^+$ cell infiltration is limited to the very narrow regions near epicardium. The majority of the myocardium is intact. On POD 4 (Fig. 7*B*), ED1$^+$ cell infiltration is still more concentrated around the pericardium regions, but the area with ED1$^+$ cells is larger, with a larger distance to the edge compared with that on POD 3. The area with ED1$^+$ cells also shows less myocardium integrity. On POD 5 (Fig. 7*C*), more ED1$^+$ cells can be found well inside the myocardium further away from the edge of the heart. On POD 6 (Fig. 7*D*) when the moderate to severe rejection is occurring, ED1$^+$ cells show aggressive infiltration throughout the inner regions of the heart with more deterioration of myocardium integrity. This temporal and spatial distributions of ED1$^+$ cells

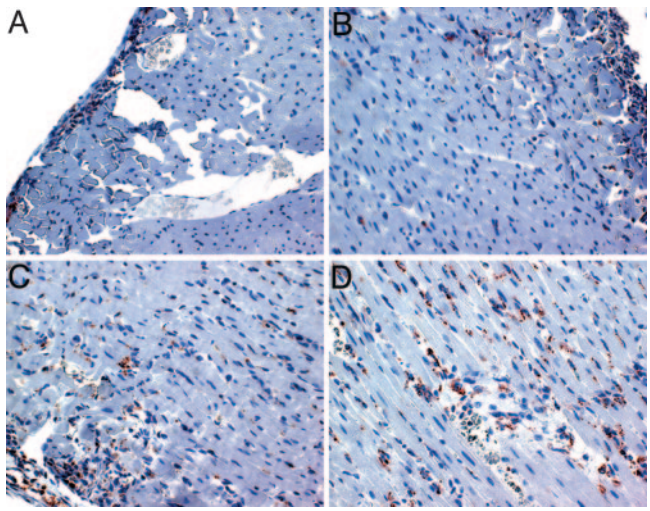

Fig. 7. Temporal progression of ED1$^+$ cell infiltration. Optical micrograph (×400 magnification) of anti-rat ED1$^+$ immunohistochemical staining sections of allograft hearts obtained on POD 3 (*A*), POD 4 (*B*), POD 5 (*C*), and POD 6 (*D*). The ED1$^+$ cells appear brown and the background is counterstained blue.

are the same regardless of iron oxide particle injection and correlate well with the MPIO-labeled cells imaged by *in vivo* MRI. This observation substantiates the conclusion that the pericardium-to-endocardium progression of MPIO-labeled macrophages observed during the rejection process is indeed showing the actual rejection phenomenon, rather than due to nonspecific artifacts. In addition, this pericardium-to-endocardium progression pattern can be used for a correct staging of acute myocardial rejection with *in vivo* MRI without needle biopsy, and thus can be potentially very useful for clinical applications.

Feasibility of Cellular Imaging of Single Cells *in Vivo*. We believe that the discrete and punctate contrast pattern observed after *in vivo* MPIO labeling could be caused by individual macrophages, despite a spatial resolution larger than that of a single cell. The local magnetic-field gradient generated by a superparamagnetic iron center can propagate as large as 50 times its radius (36). Our data (Fig. 5 *F* and *H*) indicate that there are probably several MPIO particles incorporated into each macrophage, most likely in the cytoplasm. Thus, instead of each MPIO particle, each iron-laden cell becomes a basic unit of the contrast agents. The dimension of a basic contrast-agent unit then becomes the size of a macrophage, ranging from 20 to 40 μm in diameter. In turn, the MRI-detectable effective radius of an iron-laden macrophage could approach up to 1,000–2,000 μm in diameter, well within the resolution range of *in vivo* MRI. The *in vivo* images presented here have an in-plane resolution of 156 μm. Thus, theoretically one MPIO-labeled macrophage can potentially cause signal attenuation in a volume of globe up to 6–12 pixels in diameter, even though the actual size of a labeled cell is much smaller compared with the size of an imaging voxel. Very recently, Shapiro *et al*. (37) reported that *ex vivo*-labeled primary mouse hepatocytes could migrate from spleen to liver in a mouse and be detected as single cells *in vivo* with MRI. This finding is consistent with our observation that it is possible to image single cells *in vivo* with MRI with a more sensitive contrast agent, such as MPIO.

With the smaller USPIO particles, a cell must ingest millions of particles to cause enough local field distortion to be detectable by MRI (20). This condition can be achieved with *ex vivo* labeling, but it is very challenging with *in vivo* labeling. The micrometer-sized MPIO particle is ≈35 times larger in diameter, and ≈42,875 times larger in volume, compared with that of the USPIO particle. Potentially, each MPIO particle can produce up to 40,000 times larger background attenuation. Thus, the loading of only a few MPIO particles per cell is sufficient to produce detectable signal attenuation within one imaging voxel.

Physiochemical Consideration for *in Vivo* Labeling. This report details MRI detection of single immune cells after *in vivo* labeling by direct i.v. injection of MPIOs. This method is potentially more easily applied to a clinical setting than *ex vivo* labeling of immune cells. The metabolic pathways and pathological consequences for *in vivo* MPIO-particle administration need to be further investigated. From our preliminary observation, all animals that have been injected with MPIOs seem to be healthy with no detectable behavioral or physiological alterations. Animals with isograft transplantation can live for at least 2 months after MPIO-particle administration with no obvious physiological changes. The physiochemical pathways, pharmacokinetics, and toxicity of USPIO and SPIO are well understood (25–28, 38). After USPIO or SPIO administration, iron can be found to accumulate in endosomes of Kupffer cells, the specialized macrophages in the liver, and other reticuloendothelial cells. There was transient increase in serum ferritin levels, and the administered iron eventually enters the normal iron pool of the body. It is conceivable that the iron in the MPIOs might follow the similar metabolic pathways as USPIO or SPIO particles, although the effect of the polymer coating needs further investigation.

Concluding Remarks. After the convenient *in vivo* labeling procedure, MPIO-labeled macrophages give rise to distinct punctate, MRI-detectable hypointensity, which allows noninvasive detection of myocardial rejection. The large MPIO particles result in significant MRI contrast, making *in vivo* cellular imaging of single cells possible. Once incorporated into cells, the label is very stable and allows repetitive imaging over a long period, which will be very useful for tracking cellular and developmental processes as well as for monitoring cellular therapy.

Materials and Methods

Animal Model. Inbred male Dark-Agouti (DA; RT1^{avl}) and Brown Norway (BN; RT1^{n}) rats chosen for this study were obtained from Harlan Labs (Indianapolis). At the time of surgery, they were 2–3 months of age, weighing 230 ± 20 g. All animals received humane care in compliance with the *Guide for the Care and Use of Laboratory Animals*, published by the National Institutes of Health, and the animal protocol was approved by the Carnegie Mellon University Institutional Animal Care and Use Committee.

Transplantation Model. The operative procedure for our heterotopic working-heart model has been described elsewhere (24). Allogeneic transplantation between different strains of rats (DA→BN) results in rejection, whereas syngeneic transplantation between the same strains of rats (DA→DA or BN→BN) causes no rejection. The rejection grade of the heart and lung grafts was determined histopathologically according to International Society for Heart and Lung Transplantation (22, 39) and Lung Rejection Study Group (40, 41) criteria, respectively. For the allogeneic heart grafts, mild (grade 1A or B) rejection develops by POD 3 ± 1 in our rat model, grade 2 rejection develops on POD 5 ± 1, whereas the moderate to the severe (grade 3A) rejection develops after POD 6 ± 1. All lung grafts develop severe grade 4 rejection on POD 5, whereas the severe grade 4 rejection of the transplanted heart is not manifested until after POD 7.

Contrast Agents. The MPIO particles are 0.9-μm superparamagnetic styrene-divinyl benzene inert polymer microspheres that contain a magnetite core and a fluorescein-5-isothiocyanate dye (Dragon Green) encapsulated within the cross-linked polymer sphere (Bangs Laboratories, Fishers, IN). The particles were prepared for infusion/cell labeling by washing with PBS followed by resuspension in PBS at 1.5 mg Fe/ml. Dextran-coated USPIO particles were synthesized according to the procedure described earlier (18), and the particles are ≈27 nm in size.

***In Vivo* Labeling.** MPIO or USPIO particles were administered by direct intravenous injection through a femoral venous catheter. The amount of iron injected was the same for either particle, 4.5 mg Fe/kg body weight. MPIOs are highly magnetic and sediment easily; therefore, vigorous vortexing immediately before injection and injection outside the magnetic fringe field are necessary for positive outcomes.

***Ex Vivo* Labeling.** Macrophages were isolated and purified from spleens of BN rats, then maintained in culture. The MPIOs were prepared for cell labeling by washing and resuspension in PBS with a concentration of 4 mg Fe/ml. Macrophages were labeled with MPIOs by adding 20 μl of the MPIO-PBS suspension into 10 ml of culture (1×10^7 cells per ml) before overnight incubation. After proper washing, the labeled macrophages were resuspended to desirable cell densities (1×10^6, 0.5×10^6, 0.1×10^6, 0.05×10^6 cells per ml) and embedded in 2% agarose gel.

***In Vivo* MRI.** Anesthesia was induced with isofluorane, and rats were then intubated and ventilated at a 60 strokes-per-minute rate with a 70% O_2 and 30% N_2O gas mixture and 2–2.5% isofluorane for the duration of the MRI procedure. Electrocardiogram (ECG) leads were placed on the both hind limbs of the transplanted rats to detect the heartbeat of the transplanted heart at the inguinal region. The rat core body temperature was maintained at 36.5°C ± 1°C.

MRI scans were performed with a Bruker (Billerica, MA) AVANCE DRX 4.7-T/40-cm system equipped with a 12-cm, 40-G/cm shielded gradient set. A 5.5-cm home-built surface coil was used for excitation and detection. Multislice ECG- and respiratory-gated T_2^*-weighted gradient-echo images were acquired with the following parameters: repetition time (TR) = one respiration cycle (≈1 s); echo time (TE) = 8 ms; field of view (FOV) = 3–4 cm; slice thickness = 1 or 1.5 mm; in-plane resolution = 156 μm.

MRM. After MRI evaluation, grafts were harvested and fixed in 4% paraformaldehye/1% glutaldehyde solution overnight, then stored in PBS. For MRM studies, the fixed hearts were imaged by using a Bruker AVANCE 11.7-T/89-mm system with a Micro2.5 gradient insert. High-resolution 3D images were acquired with the following parameters: TR = 500 ms; TE = 8 ms; isotropic resolution = 40 μm.

Pathological and Immunohistochemical Analysis. After MRI, the heart grafts were infused with 4% paraformaldehyde, harvested, and submitted to the Transplantation Pathology Laboratory of the University of Pittsburgh School of Medicine (Pittsburgh, PA). Paraffin-embedded 5-μm sections were subjected to hematoxylin/eosin staining for rejection grading, Perl's Prussian blue staining for the presence of iron, and immunohistochemical staining with monoclonal anti-rat ED1 antibody for staining macrophages. In addition, immunofluorescent staining was performed to further confirm the MRI results. Seven-micrometer sections of snap-frozen graft tissue were incubated with mouse monoclonal anti-rat ED1 antibody (Serotec) followed by incubation with biotinylated anti-mouse antibody and Avidin D Texas red (Vector Laboratories). Then the slices were subjected to dual-channel fluorescence microscopic examination, i.e., in green (Dragon Green) for MPIO detection and red (Texas red color) for $ED1^+$ cell detection.

We thank Dr. K.-T. Yung for making a surface coil, Mr. J. P. Suhan for performing EM, Dr. F. Lanni for providing valuable advice on fluorescence microscopy, and Ms. J. A. Horner for assistance with animals. Our research is supported by National Institutes of Health Research Grants R01EB-00318, P41EB-00197, and S10RR-15704 and Health Research Formula Funds of the Commonwealth University Research Enhancement Section of the Tobacco Settlement Act 47 (Grant ME-02-168). Y.L.W. was supported by Ruth L. Kirschstein National Research Service Award F32HL-068423. The Pittsburgh NMR Center is supported by the National Institute of Biomedical Imaging and Bioengineering as a National Biomedical Research Resource Center (P41EB-001977). A preliminary report of our results was presented at the Eighth Annual meeting of the Society for Cardiovascular Magnetic Resonance (SCMR) held on January 21–23, 2005, San Francisco.

1. Hill, J. M., Dick, A. J., Raman, V. K., Thompson, R. B., Yu, Z. X., Hinds, K. A., Pessanha, B. S., Guttman, M. A., Varney, T. R., Martin, B. J., *et al*. (2003) *Circulation* **108,** 1009–1014.
2. Cahill, K. S., Gaidosh, G., Huard, J., Silver, X., Byrne, B. J. & Walter, G. A. (2004) *Transplantation* **78,** 1626–1633.
3. Bos, C., Delmas, Y., Desmouliere, A., Solanilla, A., Hauger, O., Grosset, C., Dubus, I., Ivanovic, Z., Rosenbaum, J., Charbord, P., *et al*. (2004) *Radiology* **233,** 781–789.
4. Bulte, J. W., Duncan, I. D. & Frank, J. A. (2002) *J. Cereb. Blood Flow Metab*. **22,** 899–907.
5. Bulte, J. W., Douglas, T., Witwer, B., Zhang, S. C., Lewis, B. K., van Gelderen, P., Zywicke, H., Duncan, I. D. & Frank, J. A. (2002) *Acad. Radiol*. **9,** S332–S335.
6. Kraitchman, D. L., Heldman, A. W., Atalar, E., Amado, L. C., Martin, B. J., Pittenger, M. F., Hare, J. M. & Bulte, J. W. (2003) *Circulation* **107,** 2290–2293.
7. Walter, G. A., Cahill, K. S., Huard, J., Feng, H., Douglas, T., Sweeney, H. L. & Bulte, J. W. (2004) *Magn. Reson. Med*. **51,** 273–277.
8. Modo, M., Cash, D., Mellodew, K., Williams, S. C., Fraser, S. E., Meade, T. J., Price, J. & Hodges, H. (2002) *NeuroImage* **17,** 803–811.
9. Hoehn, M., Kustermann, E., Blunk, J., Wiedermann, D., Trapp, T., Wecker, S., Focking, M., Arnold, H., Hescheler, J., Fleischmann, B. K., *et al*. (2002) *Proc. Natl. Acad. Sci. USA* **99,** 16267–16272.
10. Anderson, S. A., Glod, J., Arbab, A. S., Noel, M., Ashari, P., Fine, H. A. & Frank, J. A. (2005) *Blood* **105,** 420–425.
11. Oweida, A. J., Dunn, E. A. & Foster, P. J. (2004) *Mol. Imaging* **3,** 85–95.
12. Rausch, M., Hiestand, P., Baumann, D., Cannet, C. & Rudin, M. (2003) *Magn. Reson. Med*. **50,** 309–314.
13. Ho, C. & Hitchens, T. K. (2004) *Curr. Pharm. Biotechnol*. **5,** 551–566.
14. Moore, A., Josephson, L., Bhorade, R. M., Basilion, J. P. & Weissleder, R. (2001) *Radiology* **221,** 244–250.
15. Genove, G., DeMarco, U., Xu, H., Goins, W. F. & Ahrens, E. T. (2005) *Nat. Med*. **11,** 450–454.
16. Bulte, J. W. & Kraitchman, D. L. (2004) *NMR Biomed*. **17,** 484–499.
17. Aime, S., Barge, A., Cabella, C., Crich, S. G. & Gianolio, E. (2004) *Curr. Pharm. Biotechnol*. **5,** 509–518.
18. Dodd, S. J., Williams, M., Suhan, J. P., Williams, D. S., Koretsky, A. P. & Ho, C. (1999) *Biophys. J*. **76,** 103–109.
19. Foster-Gareau, P., Heyn, C., Alejski, A. & Rutt, B. K. (2003) *Magn. Reson. Med*. **49,** 968–971.
20. Shapiro, E. M., Skrtic, S., Sharer, K., Hill, J. M., Dunbar, C. E. & Koretsky, A. P. (2004) *Proc. Natl. Acad. Sci. USA* **101,** 10901–10906.
21. Hinds, K. A., Hill, J. M., Shapiro, E. M., Laukkanen, M. O., Silva, A. C., Combs, C. A., Varney, T. R., Balaban, R. S., Koretsky, A. P. & Dunbar, C. E. (2003) *Blood* **102,** 867–872.
22. Winters, G. L., Marboe, C. C. & Billingham, M. E. (1998) *J. Heart Lung Transplant*. **17,** 754–760.
23. Knosalla, C. H., Hummel, M., Muller, J., Grauhan, O., Ewert, R. & Hetzer, R. (2000) *Curr. Opin. Transplant*. **5,** 118–125.
24. Wu, Y.-J. L., Sato, K., Qing, Y. & Ho, C. (2004) *Methods Enzymol*. **386,** 73–105.
25. Frank, J. A., Miller, B. R., Arbab, A. S., Zywicke, H. A., Jordan, E. K., Lewis, B. K., Bryant, L. H., Jr., & Bulte, J. W. (2003) *Radiology* **228,** 480–487.
26. Arbab, A. S., Bashaw, L. A., Miller, B. R., Jordan, E. K., Bulte, J. W. & Frank, J. A. (2003) *Transplantation* **76,** 1123–1130.
27. Arbab, A. S., Bashaw, L. A., Miller, B. R., Jordan, E. K., Lewis, B. K., Kalish, H. & Frank, J. A. (2003) *Radiology* **229,** 838–846.
28. Arbab, A. S., Yocum, G. T., Kalish, H., Jordan, E. K., Anderson, S. A., Khakoo, A. Y., Read, E. J. & Frank, J. A. (2004) *Blood* **104,** 1217–1223.
29. Josephson, L., Tung, C. H., Moore, A. & Weissleder, R. (1999) *Bioconjugate Chem*. **10,** 186–191.
30. Lewin, M., Carlesso, N., Tung, C. H., Tang, X. W., Cory, D., Scadden, D. T. & Weissleder, R. (2000) *Nat. Biotechnol*. **18,** 410–414.
31. Ahrens, E. T., Feili-Hariri, M., Xu, H., Genove, G. & Morel, P. A. (2003) *Magn. Reson. Med*. **49,** 1006–1013.
32. Zhang, Y., Dodd, S. J., Hendrich, K. S., Williams, M. & Ho, C. (2000) *Kidney Int*. **58,** 1300–1310.
33. Kanno, S., Lee, P. C., Dodd, S. J., Williams, M., Griffith, B. P. & Ho, C. (2000) *J. Thorac. Cardiovasc. Surg*. **120,** 923–934.
34. Kanno, S., Wu, Y. J., Lee, P. C., Dodd, S. J., Williams, M., Griffith, B. P. & Ho, C. (2001) *Circulation* **104,** 934–938.
35. Ye, Q., Yang, D., Williams, M., Williams, D. S., Pluempitiwiriyawej, C., Moura, J. M. & Ho, C. (2002) *Kidney Int*. **61,** 1124–1135.
36. Lauterbur, P. C., Bernardo, M. L., Jr., Menonca Dias, M. H. & Hedges, L. K. (1986) in *Proceedings of the Fifth Annual Meeting of the Society of Magnetic Resonance in Medicine* (Society of Magnetic Resonance in Medicine, Berkeley, CA) pp. 229–230.
37. Shapiro, E. M., Sharer, K., Skrtic, S. & Koretsky, A. P. (2005) *Magn. Reson. Med*., in press.
38. Jung, C. W. & Jacobs, P. (1995) *Magn. Reson. Imaging* **13,** 661–674.
39. Billingham, M. E., Cary, N. R., Hammond, M. E., Kemnitz, J., Marboe, C., McCallister, H. A., Snovar, D. C., Winters, G. L. & Zerbe, A. (1990) *J. Heart Transplant*. **9,** 587–593.
40. Yousem, S. A., Berry, G. J., Cagle, P. T., Chamberlain, D., Husain, A. N., Hruban, R. H., Marchevsky, A., Ohori, N. P., Ritter, J., Stewart, S. & Tazelaar, H. D. (1996) *J. Heart Lung Transplant*. **15,** 1–15.
41. Yousem, S. (1996) *Transplant. Proc*. **28,** 477–479.